PHYSICAL REVIEW A VOLUME 40, NUMBER 5 SEPTEMBER 1, 1989

Wetting and drying transitions at a fluid-wall interface: Density-functional theory versus computer simulation

Frank van Swol
Department of Chemical Engineering, University of Illinois, Urbana, Illinois 61801

J. R. Henderson
School of Chemistry, University of Leeds, Leeds LS2 9JT, United Kingdom
(Received 31 January 1989)

This paper reports on studies of wetting phase behavior and interfacial density profiles of square-well fluid adsorbed at a square-well wall. At a specific drying transition, a comparison is made between computer-simulation data and coarse-grained density-functional theory. The successes and failures of this comparison form the basis of a detailed discussion of the strengths and weaknesses of the two approaches, as presently implemented, and proposals are made for removing the current ambiguities. In addition, density-functional theory is used to map out the global interfacial phase behavior at bulk liquid-vapor coexistence, in terms of the fields $\{T,\epsilon_w\}$ where T denotes temperature and ϵ_w is the strength of the attractive wall-fluid interaction. Particular attention is paid to questions of statistical-mechanical consistency in the form of exact sum rules.

I. INTRODUCTION

A. Wetting transitions at simple fluid-wall interfaces

In this paper we are concerned with statistical thermodynamic transitions occurring between different states of fluid adsorption at a container wall when the bulk fluid (far from the wall) lies at liquid-vapor coexistence. For the simplest systems three states of adsorption can be envisaged: (i) complete wetting, where the adsorbed film is a macroscopic layer of liquid, (ii) partial wetting, where for a macroscopic system the adsorbed film consists of a finite layer of adsorbed liquid drops and vapor bubbles, and (iii) complete drying, where the adsorbed film is a macroscopic layer of vapor. This phase behavior can be considered to belong to a phase space consisting of two bulk thermodynamic fields, temperature (T), and chemical potential (μ), together with a set of surface "thermodynamic" fields; for example, parameters describing the strength (ϵ_w) and range (a_w) of the attractive wall-fluid interactions. Thus complete wetting occurs at high positive values of ϵ_w (strongly attractive walls), while low or negative values of ϵ_w (repulsive walls) enforce complete drying and intermediate values yield partial wetting.

In the restricted space of (T,μ,ϵ_w), the boundary between complete wetting (or complete drying) and partial wetting is a curve of first-order and/or second-order wetting (or drying) transitions lying in the (T,μ_{cc},ϵ_w) surface (where cc denotes a value at bulk liquid-vapor coexistence). Points on this curve separating first-order from second-order behavior are tricritical points.[1] In general, for appropriate values of a_w one expects to find two tricritical points, one on the drying side and one on the wetting side, separating low-temperature first-order wetting and drying transitions from second-order or so-called critical transitions at higher temperatures (up to the bulk critical point temperature). In physical systems, the study of wetting transitions is most readily envisaged as a process of varying T at fixed (ϵ_w,a_w); but see Ref. 2 for an ingenious exception. However, from the point of view of statistical mechanics it is much simpler to vary the surface fields at fixed T.

Discussions such as that given above are readily generalized to provide a comprehensive statistical thermodynamic description of interfacial phase behavior, synthesizing a huge variety of surface phenomena. Since the addition of each extra field variable increases by 1 the number of degrees of freedom relevant to the Gibbs phase rule, it is clear that interfacial systems are capable of displaying a bewildering complexity of phase behavior and associated phase transitions.[3]

B. Computer simulation of wetting transitions in fluid-wall systems

In the (T,μ_{cc},ϵ_w) surface of the space (T,μ,ϵ_w) it is clear that both wetting and drying transitions must be readily observable by varying ϵ_w at fixed T. Such a procedure is straightforwardly implemented (in principle) as a computer-simulation "experiment," as was first proposed by van Swol and Henderson.[4] In their work, the fluid was confined between two walls at a sufficient separation for the system to be able to accommodate the presence of essentially bulk liquid-vapor coexistence in planar symmetry. The method of van Swol and Henderson involves using one of the walls to enforce two-phase coexistence; e.g., by ensuring complete wetting on the far wall one can study wetting transitions at a wall-vapor interface by fixing the number of particles to fill about half the simulation box with liquid and varying the value of ϵ_w on the left-hand wall to observe the transition from partial

to complete wetting (within the restriction of the finite system size). In fact, Ref. 4 is restricted to a discussion of a drying transition, the authors' being content to establish the principle that surface phase transitions are ubiquitous in such systems and can be usefully studied by computer-simulation procedures for inhomogeneous fluids. In these procedures, partial wetting corresponds to no more than a microscopically thick layer of liquid (vapor) separating bulk vapor (liquid) from the wall. The total number of particles and the geometry of the simulation box are chosen to ensure that planar symmetry is maintained throughout the simulation. Physically, one can think of this as simulating a small area of a macroscopic system, focusing on the microscopic nature of part of a wall-drop or a wall-bubble interface; e.g., a transition to complete drying corresponds to vapor "pushing" the liquid drop away from the wall. Note that here, a first-order transition is not reversible as it would be in a macroscopically sized system.

A more extensive simulation study, including both wetting and drying behavior, has since been undertaken by Sikkenk *et al.*,[5] using a special-purpose computer designed for the study of models involving Lennard-Jones interactions. This work uses symmetric boundary conditions, namely, the fluid is confined between two identical walls. Nevertheless, the finite size of the simulation box means that partial wetting states correspond to nonsymmetric density profiles (liquid adsorbed on one wall and vapor adsorbed on the other). A wetting or drying transition, obtained by varying ϵ_w identically at both walls, is then a transition to a symmetric profile. However, Ref. 5 has proved to be controversial because hardware restrictions forced Sikkenk *et al.* to construct their walls from a small number of rows of heavy Lennard-Jones atoms. This resulted in the surface free energy being dominated by an enormous surface stress contribution (i.e., the layers of solid atoms forming the walls were under tension), but, nevertheless, in calculating contact angles Ref. 5 ignored this surface stress by assuming it to be invariant with regard to the nature of the adsorption (i.e., assuming the tension of the stressed outer solid layers to be exactly the same for both the wet and dry wall).[6]

In this paper, we compare the molecular-dynamics (MD) computer-simulation results of van Swol and Henderson[4] with density-functional calculations. This, we believe, is the first such direct comparison concerning the ability to describe a wetting or drying transition. For the study of surface phase transitions, neither brute-force computer simulation nor coarse-grained density-functional theory can be said to be so well understood that it can be used to directly test the other method. Instead, this study contributes more or less equally to further understanding of the merits and problems of both procedures. Briefly, the weak link in density-functional theory is the uncertain connection between the chosen functional and the underlying model Hamiltonian one is aiming to study, while the most uncertain aspects involved in computer-simulation studies of phase transitions arise from restrictions on the amount of computational resources.

The molecular-dynamics simulations of Ref. 4 are based on a classical Hamiltonian with impulsive forces; in particular, the potential used is

$$\sum_{\substack{i\\ i<j}}\sum_{j} u(r_{ij})+\sum_{i} v(z_i)\ , \tag{1a}$$

where

$$u(r)=\begin{cases}\infty, & r<\sigma\\ -\epsilon, & \sigma<r<3\sigma/2\\ 0, & r>3\sigma/2\end{cases} \tag{1b}$$

$$v(z)=\begin{cases}\infty, & z<0,\quad z>L_z\\ -\epsilon_w, & 0<z<\sigma/2\\ 0, & \text{otherwise}\end{cases} \tag{1c}$$

and periodic boundary conditions were implemented in the XY plane. The hard-wall boundary at L_z ensured the presence of liquid-vapor coexistence because a hard wall is completely dry;[7] i.e., by equilibrating from a half-filled initial configuration the system is forced to fill the right-hand side with vapor. The drying transition was located by lowering ϵ_w in steps, equilibrating after each step, until the density profile corresponded to a liquid film sandwiched between two thick layers of vapor. The transition at the left-hand wall, between a damped oscillatory wall-liquid profile and a completely dry wall, occurred rapidly on the scale of ϵ_w. From this and related observations it was concluded that the drying transition was most likely first order, but since the sharpness of a transition cannot be arbitrarily tested by computer simulation, it is not possible to rule out rapid second-order behavior.[8] The simulation data available from Ref. 4 include contact angles, density profiles, and free-energy profiles.

C. Coarse-grained density-functional theory

Formally, it can be shown that for Hamiltonians of the class (1), the exact grand potential is given by the solution of the minimization with respect to density fluctuations of some functional of the one-body density profile $\rho(\mathbf{r})$.[9] In practice, the link with the Hamiltonian is fudged because one is forced to work with some phenomenological functional. To successfully describe the structure of a wall-liquid interface it is essential to be able to accommodate strong oscillatory behavior in the density profile. On the other hand, the grand potential should not be strongly influenced by structure that is periodic on the scale of a molecular diameter. Thus workers have proposed introducing a coarse-grained density profile $\bar{\rho}[\rho(\mathbf{r})]$, a functional of the full profile, and treating the grand potential as primarily a functional of $\bar{\rho}$.[10] Some very general theories of this type have been proposed.[11–13] To date, almost all the effort has been put into hard-core contributions to the free-energy functional. The attractive fluid-fluid interactions can in principle be treated on the same sophisticated footing, but in practice the lack of explicit knowledge of pair correlations in non-hard-sphere fluids has led to the adoption of simple mean-field treatments. Here, the best one can do is some sort of liquid-state per-

turbation theory,[13(b)] so the usual choice has been to adopt the simplest such approach:

$$\Omega = F_{\rm HS}^{\rm ex}[\bar\rho] + \tfrac{1}{2}\int d1\int d2\,\rho(1)\rho(2)u_a(r_{12}) + kT\int d1\,\rho(1)\{\ln[\Lambda^3\rho(1)]-1\} + \int d1\,\rho(1)[v(1)-\mu]\ , \tag{2a}$$

where $\Lambda \equiv (h^2/2m\pi kT)^{1/2}$ and

$$u_a(r) = \begin{cases} u(r_{\rm min}), & r < r_{\rm min} \\ u(r), & r > r_{\rm min} \end{cases}$$

[$u(r) \geq u(r_{\rm min})$ defines $r_{\rm min}$]. In numerical evaluations, the hard-sphere (HS) free-energy functionals used to date all belong to a class known as the weighted-density approximation (WDA):

$$F_{\rm HS}^{\rm ex}[\bar\rho] = \int d1\,\rho(1)\Delta\psi_{\rm HS}(\bar\rho(1))\ , \tag{2b}$$

$$\bar\rho(1) \equiv \int d2\,\rho(2)w(12,\bar\rho(1))\ , \tag{2c}$$

where $\Delta\psi_{\rm HS}(\rho)$ denotes the excess free energy per particle in a homogeneous hard-sphere system (of density ρ) and $w(12,\rho)$ is the nonlocal weight function (which in the WDA is itself a function of ρ).

The implementation of the density-functional theory defined by (2) proceeds by invoking the condition for thermodynamic equilibrium $\delta\Omega/\delta\rho = 0$; i.e.,

$$kT\ln[\Lambda^3\rho(1)] + [v(1)-\mu] + \int d2\,\rho(2)u_a(12) + \Delta\psi_{\rm HS}(\bar\rho(1)) + \int d2\,\rho(2)\Delta\psi'_{\rm HS}(\bar\rho(2))\frac{\delta\bar\rho(2)}{\delta\rho(1)} = 0 \tag{3a}$$

together with

$$\frac{\delta\bar\rho(1)}{\delta\rho(2)} = \frac{w(12,\bar\rho(1))}{1-\int d3\,\rho(3)w'(13,\bar\rho(1))}\ . \tag{3b}$$

Here, the prime denotes the density derivative $\partial/\partial\bar\rho$. In homogeneous bulk fluid (2c) and (3b) reduce to

$$\int d\mathbf{r}\,w(r,\rho) = 1, \quad \frac{\delta\bar\rho(1)}{\delta\rho(2)} = w(r_{12},\rho)\ , \tag{4a}$$

and thus (3) assumes a modified van der Waals bulk equation of state:

$$\Delta\psi(\rho) = \Delta\psi_{\rm HS}(\rho) - \tfrac{1}{2}\alpha\rho\ ,$$
$$\mu(\rho) = kT\ln(\Lambda^3\rho) + [\rho\Delta\psi(\rho)]'\ , \tag{4b}$$
$$\alpha = -\int d\mathbf{r}\,u_a(r)\ .$$

Since the bulk density and equation of state are imposed boundary conditions on the density-functional algorithm, we can rewrite (3a) as

$$\rho(1)/\rho = \exp\{-[v(1)/kT] + c^{(1)}(1) - c_b^{(1)}\}\ , \tag{5a}$$

where the only quantity requiring numerical evaluation is the one-body direct correlation function, $c^{(1)}(1)$,

$$-kTc^{(1)}(1) = \frac{\delta F^{\rm ex}}{\delta\rho(1)} = \Delta\psi_{\rm HS}(\bar\rho(1)) + \int d2\,\rho(2)\Delta\psi'_{\rm HS}(\bar\rho(2))\frac{\delta\bar\rho(2)}{\delta\rho(1)} + \int d2\,\rho(2)u_a(12)\ . \tag{5b}$$

The value in bulk fluid is given by the equation of state

$$-kTc_b^{(1)} = (\rho\Delta\psi)' = \mu^{\rm ex}(\rho)\ . \tag{5c}$$

Taking further functional derivatives of 5(b) generates the hierarchy of direct correlation functions defined by the WDA functional,

$$c^{(s)}(1,2,\ldots,s) \equiv \frac{\delta^{s-1}c^{(1)}(1)}{\delta\rho(2)\cdots\delta\rho(s)}\ . \tag{6}$$

Since feasible criteria for the choice of weight function are restricted to comparison with bulk fluid properties, it follows that one should restrict the choice of weight function to a homogeneous form, $w(r_{12},\bar\rho(1))$. Here, we are forced to explicitly consider pair correlations, because the bulk fluid one-body direct correlation function and all its density derivatives, see (5c) and (6), are determined by the equation of state. Accordingly, it is natural to generate physically sensible criteria for the weight function by requiring a good description of the hard-sphere two-body direct correlation function.[14] One helpful property of WDA theory is that the exponential form of (5a) essentially guarantees a positive definite density profile. Exceptions could arise if the right-hand side of (5a) contained a factor of the form $\exp[\ln f(1)]$, since negative $f(1)$ would correspond to negative $\rho(1)$. To date, this problem has only been encountered when using the primitive van der Waals equation of state,

$$-\Delta\psi_{\rm HS}(\bar\rho)/kT = \ln(1-\bar\rho v)\ ,$$

where v is the hard-sphere excluded volume; i.e., unphysical negative densities arise if $\bar\rho v > 1$.[15]

The particular WDA density-functional theory used in this work is due to Tarazona.[14] In fact, we are indebted to Dr. Tarazona for supplying us with a version of his numerical program written for the specific case of Yukawa fluid-fluid interactions and an exponential wall-fluid potential. We were required to make extensive changes to enable the program to accommodate the discontinuous square-well potentials of our underlying model (1). The choice of weight function adopted by Tarazona is a three-term virial expansion

$$w(r,\rho) = w_0(r) + \rho w_1(r) + \rho^2 w_2(r)\ , \tag{7}$$

with the coefficients $w_i(r)$ extracted from a fit to the corresponding virial expansion of the Percus-Yevick hard-sphere two-body direct correlation function.[16] The zeroth-order term is the normalized step function,

$$w_0(r) = \begin{cases} 3/4\pi\sigma^3, & r < \sigma \\ 0, & r > \sigma \end{cases} \tag{8}$$

where σ is the hard-sphere diameter. The weak-gas limit result for the generalized WDA applied to an arbitrary

pair-potential fluid [i.e., combining the first two terms on the right-hand side of (2a) in the WDA form] is readily shown to be

$$w_0(r)=\frac{e^{-u(r)/kT}-1}{\int d\mathbf{r}(e^{-u(r)/kT}-1)} . \tag{9}$$

Curtin and Ashcroft[13(a)] have expressed surprise that WDA theory based on the low-density expansion (7) should yield such good results for the density profile and free energy of a dense inhomogeneous liquid. Presumably, part of the reason for this is because it is possible to accurately fit the two-body direct correlation function of dense hard-sphere fluid with a three-term density expansion. In fact, Tarazona empirically modifies the form of $w_2(r)$ to obtain a good fit at all liquid densities. Furthermore, the calculated free energy and density profile can be expected to be much less sensitive to the choice of weight function than a pair correlation function (cf. Sec. I D below).

D. Statistical-mechanical sum rules

In the all-field phase space of (T,μ,ϵ_w,a_w) the statistical-mechanical sum rules obtained by isothermal functional differentiation of the partition function with respect to the remaining field variables (μ,ϵ_w,a_w) comprise a generalized compressibility route to the statistical mechanics of wall-fluid systems. For example, van Swol and Henderson[4] discuss sum rules for derivatives of the contact angle (θ);

$$\Omega_{LV}^{(s)}\cos\theta\equiv\Omega_{WV}^{(s)}-\Omega_{WL}^{(s)} , \tag{10}$$

where the superscript (s) denotes a surface excess quantity, defined with respect to a Gibbs dividing surface that is not dependent on the surface field parameters (ϵ_w,a_w), and the subscripts label the actual interface involved (note, $\cos\theta=-1$ corresponds to complete drying and $\cos\theta=+1$ to complete wetting). In particular, in planar symmetry one has the sum rule

$$\gamma_{LV}\frac{\partial\cos\theta}{\partial\epsilon_w}=\bar{V}_{WV}-\bar{V}_{WL} , \tag{11a}$$

where $\gamma_{LV}\equiv\Omega_{LV}^{(s)}/A$, A is the area of a wall, and

$$\bar{V}_{ij}\equiv\int_{z_i}^{z_j}dz\,\rho(z)\frac{\partial v(z,\epsilon_w,a_w)}{\partial\epsilon_w} . \tag{11b}$$

Many more compressibility route sum rules, none of which explicitly involves the fluid-fluid interactions, are also discussed in Ref. 4. In addition, it has been shown that such sum rules severely constrain the nature of continuous wetting transitions.[17]

Also available is a complementary set of sum rules involving gradients of the fluid-fluid potential, the most well known being the condition for hydrostatic equilibrium, or force balance. Here, it is convenient to rewrite the force-balance condition by introducing a pressure tensor;[18] namely, in planar symmetry

$$p_N'(z)=-\rho(z)v'(z) , \tag{12}$$

where $p_N(z)$ denotes the normal component of the pressure tensor. By integrating (12) across a boundary wall to a value of z beyond the range of the wall field $v(z)$, we obtain a sum rule linking the bulk pressure (p) with an integral over the surface forces:

$$p=-\int_{-\infty}^{z_b}dz\,\rho(z)v'(z) . \tag{13a}$$

To interpret (13a) in the presence of discontinuous external fields (and hence a discontinuous density profile), it is useful to note from graph theory that the function $n(z)$, defined by

$$\rho(z)\equiv n(z)\exp[-v(z)/kT] , \tag{13b}$$

is continuous everywhere (n is a one-body y function). In planar symmetry, a transverse component of the pressure tensor can be regarded as a grand potential density (or rather, minus this quantity). So, a surface excess grand potential of a planar wall-fluid system can be expressed as

$$\Omega^{(s)}/A=\int_{-\infty}^{z_b}dz[p\Theta(z)-p_T(z)] , \tag{14}$$

where $\Theta(z)$ is the unit step function and we have chosen to denote the origin ($z=0$) by the position of the Gibbs dividing surface. Sum rule (14) was used in Ref. 4 to measure contact angles, as defined by (10). Pressure tensor component profiles were also collected.

An important criterion for the physical relevance of an approximate numerical theory, such as density-functional theory, is the level of consistency with statistical-mechanical sum rules; i.e., density-functional theory cannot guarantee to preserve the statistical identities of a true Hamiltonian-based theory. The natural statistical-mechanical framework of density-functional theory is the compressibility route. However, it is still possible to ask for consistency with hydrostatic equilibrium because in statistical mechanics one can transform Eq. (12), or its generalization to arbitrary symmetry, directly into the gradient of Eq. (5a).[19] That is, in a single-component system the constancy of chemical potential is equivalent to hydrostatic force balance. In particular, a density-functional theory of a planar wall-fluid interface will exactly satisfy sum rule (13a), provided that

$$p=kT\rho-kT\int_{-\infty}^{z_b}dz\,\rho(z)c^{(1)\prime}(z) . \tag{15}$$

In WDA theory the last term of (15) is given by (5b) in planar symmetry; i.e.,

$$\begin{aligned}&\int_{-\infty}^{z_b}dz\,\rho(z)\frac{d}{dz}\Delta\psi_{\mathrm{HS}}(\bar{\rho}(z))\\&\quad+\int d2\,\rho(z_2)\Delta\psi_{\mathrm{HS}}'(\bar{\rho}(z_2))\int_{-\infty}^{z_b}dz_1\rho(z_1)\frac{d}{dz_1}\frac{\delta\bar{\rho}(2)}{\delta\rho(1)}\\&\quad+\int d2\,\rho(z_2)\int_{-\infty}^{z_b}dz_1\rho(z_1)\frac{d}{dz_1}u_a(r_{12}) .\end{aligned} \tag{16a}$$

Here, we can integrate by parts in the second term and make use of the functional calculus identity

$$\begin{aligned}\bar{\rho}'(z_2)&=\int d1\,\rho'(z_1)\frac{\delta\bar{\rho}(2)}{\delta\rho(1)}\\&=\int_{-\infty}^{z_b}dz_1\rho'(z_1)\int d\mathbf{s}_{12}\frac{\delta\bar{\rho}(2)}{\delta\rho(1)} .\end{aligned}$$

Together with (4a), this reduces the first two terms of (16a) to

$$\rho\int d2\,\rho(z_2)\Delta\psi'_{\rm HS}(\bar{\rho}(z_2))w(r_{12},\rho;z_1=z_b) = \rho^2\Delta\psi'_{\rm HS}(\rho)\ . \quad (16b)$$

Furthermore, the final term in (16a) is readily evaluated to be $-\rho^2\alpha/2$; i.e., (16a) reduces to

$$\rho^2\Delta\psi'_{\rm HS}(\rho)-\rho^2\alpha/2=p-kT\rho\ , \quad (16c)$$

as required. Thus every WDA density-functional theory satisfies, by construction, sum rule (13a) expressing force balance integrated across the interfacial region. For wall-fluid systems this consistency often places strong constraints on the density profile in the interfacial region, indicating that WDA theory is likely to be especially successful in predicting density-profile structure. It also suggests that the one-body density is insensitive to the choice of weight function, in contrast to the situation with higher-order correlation functions.

The ability of WDA theory to successfully handle discontinuous density profiles arises from the fact that $\bar{\rho}(z)$ and hence $c^{(1)}(z)$ are continuous functions, even across a hard wall. For example, consider a system with fluid occupying the space $z>0$, bounded by a hard wall. Then, the derivation leading from (16a) to (16b) has assumed

$$\int_{-\infty}^{z_b} dz\,\rho(z)\frac{d}{dz}\Delta\psi_{\rm HS}(\bar{\rho}(z))=\int_0^{z_b} dz\,\rho(z)\frac{d}{dz}\Delta\psi_{\rm HS}(\bar{\rho}(z))\ .$$

This is fine in the context of WDA theory, but breaks down in local-density-functional theory because $\bar{\rho}(z)$ reduces to $\rho(z)$. That is, the failure of local-density-functional theory to satisfy force-balance consistency in discontinuous wall-fluid systems arises from unphysical discontinuities in the one-body direct correlation function. This conclusion is also interesting in conjunction with (5a) and (13b); i.e., WDA theory preserves the continuous nature of the one-body y function, $n(z)$, whereas this important statistical-mechanical property is violated by local-density-functional theories applied to systems with discontinuous wall-fluid potentials. In the latter case, further functional differentiation of $c^{(1)}$ to yield higher-order compressibility route sum rules, see (6), must also propagate this inconsistency. In contrast, for any reasonable choice of weight function WDA theory is a self-consistent theory, in that its construction guarantees consistency with statistical-mechanical sum rules derivable by successive functional differentiation of the grand potential.

II. RESULTS

A. Wall-fluid density profiles

Well inside the partial wetting region, the numerical density-functional procedure is straightforward for both wall-liquid and wall-vapor systems. We found that 40–60 iterations (with a mixing parameter of 0.1)[14] starting from any reasonable profile was sufficient to generate a stable equilibrium profile. Sum rule (13a) proved to be of great value as a measure of the amount of numerical error. That is, for our square-well system (1) any deviation from the integrated force-balance condition

$$n(\sigma/2)-p/kT=[n(\sigma/2)-n(0)]e^{\epsilon_w/kT} \quad (17)$$

had to have arisen from numerical error. As a percentage of the bulk liquid density, this numerical error could readily be kept below 0.1% except close to a wetting transition where more complex numerical procedures were required (see Sec. II C below). In Figs. 1–3 we present a comparison of the density-functional profiles with the simulation data of Ref. 4. The simulation systems belong to the isotherm $kT/\epsilon=1$, which lies about halfway between the triple-point and critical-point temperatures, and yielded a saturated bulk liquid density of $\rho\sigma^3=0.648\pm0.004$. The crudity of the density-functional equation of state (4b) prevents a truly direct comparison with the simulation model; i.e., at the same temperature the bulk liquid density is lower ($\rho\sigma^3=0.602$). We chose to make the comparison at slightly unequal temperatures in order to enforce agreement between the values for the bulk liquid densities. In this way, we find that the closest approximation to the simulation systems is a density-functional isotherm at $T/T_c=0.738$; T_c denotes the bulk critical temperature.[20] The density-functional values of ϵ_w are chosen to keep the comparison at equal values of ϵ_w/kT; cf. (13b) and (17). The agreement shown in Figs. 1 and 2 is remarkable; clearly WDA theory is an exceptionally accurate route to the density profiles of moderately wet wall-fluid interfaces. The only discrepancy that one can observe in Figs. 1 and 2 is that the oscillatory structure beyond the range of the wall field is slightly stretched in the case of the density-functional profiles. This effect has previously been observed by Tarazona, in systems of hard-sphere fluid at a hard wall, who suggested that the cause lies in a suppression of transverse correlations inherent in the choice for the symmetry of the weight function; $w(\mathbf{r}_1,\mathbf{r}_2,\bar{\rho}(\mathbf{r}_1))\to w(r_{12},\bar{\rho}(z_1))$.[14] The comparison at $\epsilon_w/kT=1$ shows that the simulation data are

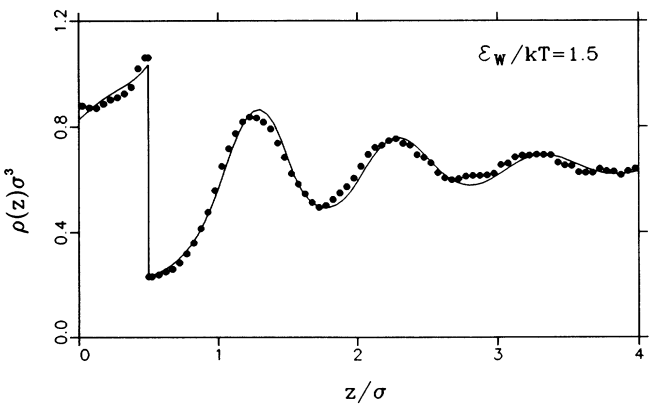

FIG. 1. Density profiles of square-well fluid in the region of a square-well wall for $\epsilon_w/kT=1.5$. Comparison of WDA density-functional theory (solid curve) with MD simulation data from Ref. 4 (points).

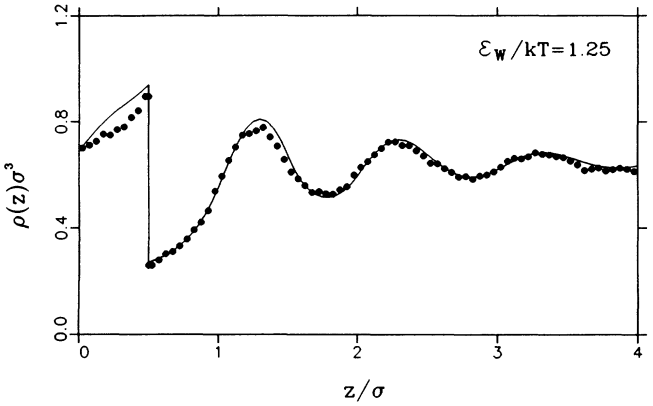

FIG. 2. As in Fig. 1, but for $\epsilon_w/kT=1.25$.

significantly closer to the drying transition than our density-functional theory predicts. Thus density-functional theory and simulation differ significantly on the position of the drying transition (see Sec. II B). Furthermore, this discrepancy may even extend to the order of the drying transition (see Sec. II C). For completeness, we display in Figs. 4 and 5 the full sets of wall-liquid and wall-vapor profiles generated by the density-functional theory when mapping out the $T/T_c=0.738$ isotherm.

B. Interfacial phase behavior

The contact angles obtained from our WDA density-functional theory applied to wall-liquid, wall-vapor, and liquid-vapor interfaces are shown in Fig. 6, for three representative isotherms. The symbols label the actual systems studied, including the positions of the wetting and drying transitions. In Fig. 7 we give the comparison with sum rule (11); i.e., between the slopes of the curves in Fig. 6 and the values of

$$\frac{kT_c}{\gamma_{LV}}\int_0^{\sigma/2} dz[\rho_{WL}(z)-\rho_{WV}(z)] \ . \tag{18}$$

Deviations from sum rule (11) can arise from two sources:

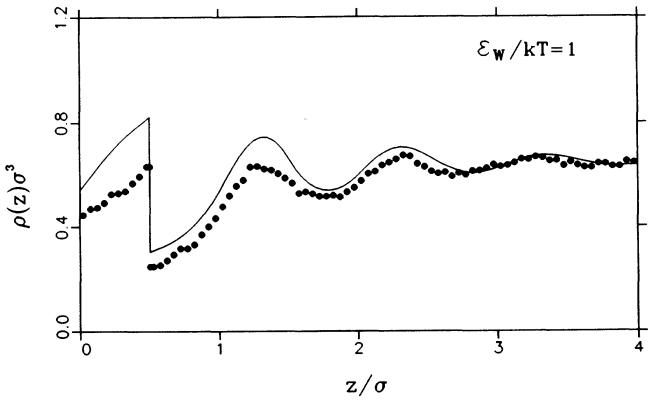

FIG. 3. As in Fig. 1, but for $\epsilon_w/kT=1$.

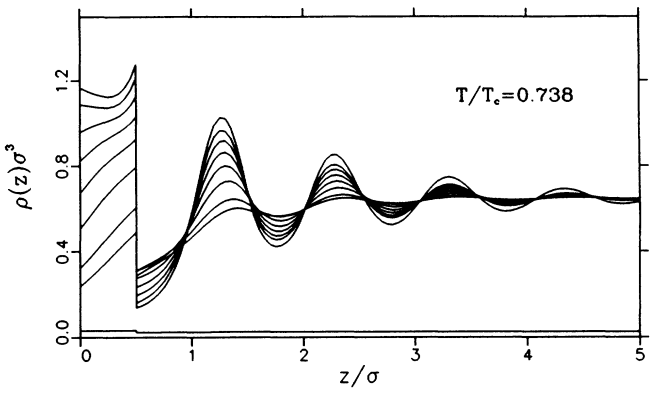

FIG. 4. Wall-liquid density profiles in the interfacial region, from WDA density-functional theory, along the isotherm $T/T_c=0.738$. The partial wetting profiles correspond to $\epsilon_w/kT_c=0.4$, 0.5, 0.7, 0.9, 1.1, 1.3, and 1.5. The remaining two curves show complete drying and complete wetting. Within the peaks, the profiles are ordered with respect to ϵ_w; i.e., the higher ϵ_w, the higher the peak.

(i) numerical errors in carrying out the density-functional algorithm and (ii) errors arising from the fit to the $\cos\theta$ data. The latter is clearly responsible for the discrepancy close to the wetting transition of the lowest-temperature isotherm (i.e., there are insufficient data points to fit the rapidly changing slope). In addition, for the same amount of iterations, numerical error is greatest close to the wetting transition, because here the equilibrium density profiles are more structured. Nevertheless, particularly for the isotherm of direct interest to the MD simulation results, Fig. 7 confirms the absence of significant numerical error arising from our numerical procedure, both in the surface free energies (contact angles) and in the density profiles [see (18)]. The density profiles were also tested by confirming consistency with sum rule (17), to a high level of accuracy. A direct measure of the numeri-

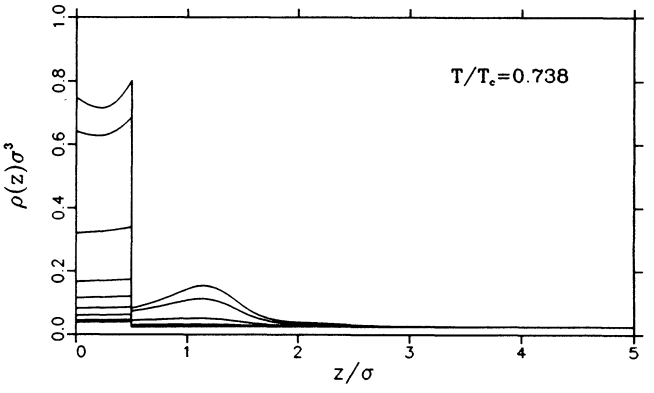

FIG. 5. Partial wetting wall-vapor density profiles from WDA density-functional theory, along the isotherm $T/T_c=0.738$. The top curve shows the partial wetting wall-vapor profile at the first-order wetting transition. The other profiles correspond to $\epsilon_w/kT_c=0.4$, 0.5, 0.7, 0.9, 1.1, 1.3, 1.5, and 1.65.

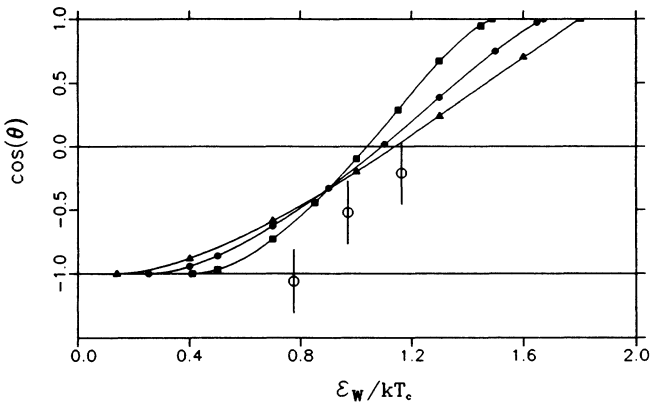

FIG. 6. Cosine of the contact angle as a function of the strength of wall-fluid attractive potential. Density-functional theory results are plotted for three representative isotherms: ■, $T/T_c=0.93$; ●, $T/T_c=0.738$; and ▲, $T/T_c=0.64$. The curves through the symbols show fits to a ratio of two polynomials, used in Fig. 7. The open circles with vertical error bars show the MD simulation data of Ref. 4, corresponding to the same bulk liquid density as the $T/T_c=0.738$ density-functional isotherm. The simulation data also involve a small horizontal error arising from imprecise knowledge of T_c, but this is no bigger than the size of our plotted symbol.

cal stability is obtained by monitoring the change in grand potential with the number of iterations. Numerical instabilities brought about by an inappropriate choice of mixing parameter will first manifest themselves as an increase in the grand potential functional. Furthermore, one always ensures that the change in grand potential between successive iterations has fallen to a sufficiently low value by the end of an iteration run.

Figure 8 displays the wetting and drying phase diagram obtained from our density-functional theory (ap-

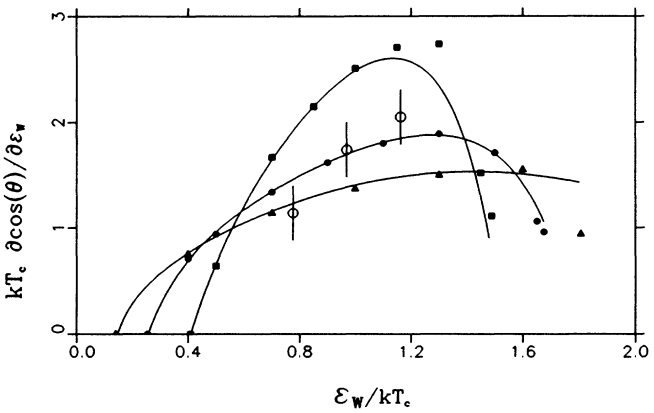

FIG. 7. The derivative with respect to the strength of the wall-fluid attractive potential, of cosine of the contact angle. The symbols denote predictions of sum rule [(11) and (18)], for the same systems plotted in Fig. 6. The curves associated with the density-functional data show the comparison with derivatives of the $\cos\theta$ fits plotted in Fig. 6. All three density-functional isotherms end at first-order wetting transitions and at second-order drying transitions.

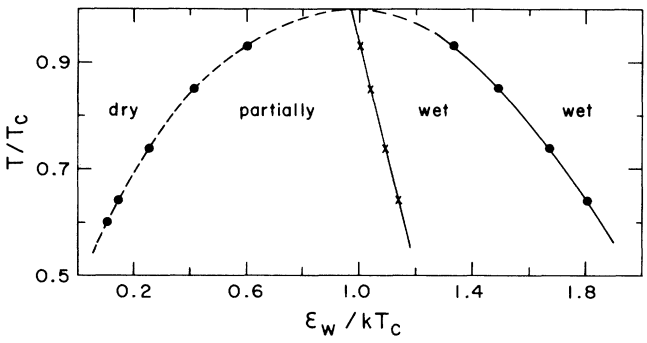

FIG. 8. Surface phase diagram for the interface between a square-well wall and square-well fluid at bulk liquid-vapor coexistence. The symbols label WDA density-functional calculations. The wetting and drying transition lines are drawn as a guide to the eye (particularly near T_c) and we have distinguished between first-order wetting (solid curve) and second-order wetting and drying transitions (dashed curve). The straight line though the data in the middle of the partial wetting region denotes a contact angle of $\pi/2$.

plied to a wider range of temperatures than shown in Figs. 6 and 7). Here, the curve through the points (which label the actual systems studied) is just a guide to the eye, in contrast to the fitted curves plotted in Fig. 6. Also shown in Fig. 8 are the values corresponding to the midpoint of the partial wetting region; i.e., defined by $\cos\theta=0$. Interestingly, in (T,ϵ_w) space, $\cos\theta=0$ defines a remarkably straight line. In fact, we did not detect any deviation from this straight line over the entire physically relevant temperature range corresponding to liquid-vapor coexistence ($0.55<T/T_c<1$). If we use this line to define the origin of the surface field ($h_1=0$) then a parabolic shape of the wetting and drying transition curve ($\cos\theta=\pm1$) in the region of the bulk critical temperature would correspond to

$$h_1(\cos\theta=\pm1)\sim t^{1/2},\quad t\equiv1-T/T_c\ . \tag{19}$$

The comparison with the MD simulation results shown in Fig. 6 indicates that our particular WDA density-functional theory cannot quite reproduce the phase behavior of the underlying Hamiltonian, even deep inside the partial wetting region. The slope of the $\cos\theta$ isotherm at $T/T_c=0.738$ is in good agreement (see also Fig. 7) but all the density-functional isotherms in Fig. 6 lie to the left of the simulation results. In particular, by considering the values of ϵ_w at $\cos\theta=0$ one can remove any error arising from the mismatch in the liquid-vapor surface tensions [see (10)]. Accordingly, we note from Fig. 6 that there is no temperature (or saturated liquid density) for which the density-functional theory would fit the true position of the midpoint of the partial wetting region at $kT=\epsilon$. This arises because the wall-liquid interfacial grand potentials predicted by our density-functional theory are consistently lower than the measured values, even for systems such as the one featured in Fig. 1 where the density profile shows an almost perfect match to the simulated profile. Presumably one is paying a price for the crude manner in which attractive fluid-fluid interac-

tions are taken into account by the functional (2). For wall-fluid interfaces involving significant packing structure, it is perhaps reasonable to expect that attractive fluid-fluid interactions will have less effect on the density profile than on the interfacial free energy. Before concluding this discussion of surface grand potentials in the partial wetting region, it is prudent to inquire if density-functional theory confirms the validity of an approximation used to generate the simulation results. Namely, in Ref. 4, which confines attention to the drying side of the phase diagram, it was assumed that $\Omega_{\mathrm{WV}}^{(s)}$ could be calculated from a weak-gas limit to an exact sum rule for the surface grand potential, without inducing significant loss of accuracy in the measured contact angle. This then avoided the need for undertaking simulations of wall-vapor interfaces in the partial drying region. When we tested this procedure on our corresponding density-functional systems,[21] it was found to be an accurate approximation throughout the entire partial drying region; in particular, for the $T/T_c=0.738$ isotherm the error in the wall-vapor surface grand potential is less than 5% for all $\cos\theta<0$. Thus our density-functional theory vindicates the method adopted in Ref. 4 to study the wetting behavior of partially dry systems, at the temperature of interest.

C. Wetting and drying transitions

For all three isotherms plotted in Figs. 6 and 7, density-functional theory yields a first-order wetting transition and a second-order drying transition. Second-order behavior corresponds to continuous changes in adsorption and in other field derivatives of the grand potential, so that in Fig. 7 the continuous nature of the drying transitions is evidenced by the fact that $\partial\cos\theta/\partial\epsilon_w$ tends smoothly to zero at the transition points. In contrast, at the first-order wetting transitions the slopes of the $\cos\theta$-versus-ϵ_w isotherms change discontinuously. In the neighborhood of a wetting or drying transition, the WDA density-functional procedure needs to be modified in order to accommodate the large changes in adsorption. The approach pioneered by Tarazona and Evans[22] is based on a separation of "time" scales between the rapid convergence of local wall-fluid structure and the slow convergence towards an equilibrium involving a substantially different amount of adsorption. In this way, the behavior of the grand potential functional at nonequilibrium values of the adsorption can be mapped out, directly analogous to following a van der Waals loop across a mean-field bulk liquid-vapor phase transition. In practice, the numerical procedure is split up into a series of iteration runs, each run beginning from an initial profile corresponding to a different adsorption (i.e., film thickness). Each run rapidly converges towards local equilibrium (40 iterations at a mixing parameter of 0.1 is ample) without significantly altering the film thickness. Instead of continuing to iterate towards the absolute minimum one simply starts again at a different thickness, thereby obtaining a density profile and a grand potential belonging to a particular adsorption. The true equilibrium thickness is of course defined by the global minimum of the grand potential. At a first-order wetting transition our grand potential displays classic mean-field behavior involving a double minimum, one minimum at a finite adsorption and the other at infinite adsorption, separated by a barrier. On either side of such a transition the barrier begins to shrink in size, but persists for some distance. The height of the barrier at the transition is a measure of the first-order nature of the transition. In an approach to a tricritical point, where the first-order behavior becomes second order, the barrier height will shrink continuously to zero. In the neighborhood of a second-order wetting transition there is never more than one turning point in the grand potential as a function of film thickness. In our program, initial profiles for wall-vapor systems containing an adsorbed film of liquid were obtained by using a tanh function (involving the width of the liquid-vapor profile) to smoothly match the relevant wall-liquid profile to bulk vapor, at chosen values of the film thickness. The same approach was also used near a drying transition. To locate the precise position of a wetting or drying transition we calculated the grand potential (Ω) for a large number of initial thicknesses (i.e., adsorptions, Γ) at various values of ϵ_w on either side of the transition. The shape of the $\Omega(\Gamma)$-versus-Γ curves told us the order of the transition and the behavior of the global minima could readily be interpolated to accurately pinpoint the positions of the transitions. The sizes of the systems were taken to be the smallest compatible with negligible finite-size effects; i.e., compatible with the requirement that doubling the length of the system did not significantly alter the numerical results (e.g., for the $T/T_c=0.738$ isotherm we used a box length of 10σ; i.e., everything to the right of $z=10\sigma$ was treated as bulk fluid).

The phase behavior at wall-vapor interfaces summarized by the right-hand side of Fig. 8 is of the generic form originally proposed for simple wall-fluid systems;[1] namely, first-order wetting transitions are found at low temperatures but at some temperature below the bulk critical temperature the behavior switches to second order. The point on the phase diagram of Fig. 8 at which this change in the nature of the wetting transitions is located can be regarded as a tricritical point. In a mean-field density-functional theory, such a tricritical point can be defined by following the gradual disappearance of the barrier in the grand potential functional at positions along the first-order section of the transition curve (i.e., by observing the disappearance of a van der Waals loop). Our density-functional data for the barrier height are plotted in Fig. 9. Clearly, an accurate determination of the tricritical point would be very time consuming because of the strong curvature displayed by the barrier heights as the tricritical point is approached. In addition, our numerical method is not easily suited to measuring barrier heights smaller than about $10^{-5}kT_c$. Fortunately, we can get an idea of the size of the extrapolation involved, from the detailed analytic analysis published by Aukrust and Hauge,[23] for a highly simplified density-functional theory concerning films of Yukawa fluid adsorbed on an exponential wall. In particular, Fig. 4 of Ref. 23 indicates that in our temperature region one

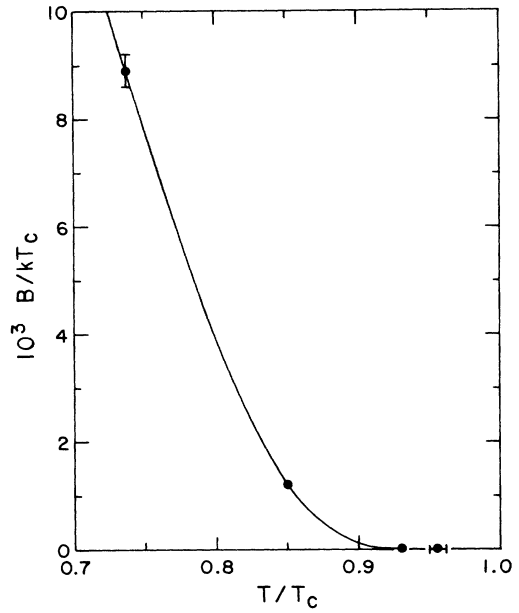

FIG. 9. Density-functional theory data for the grand potential barrier height (B) at first-order wetting transitions, in the approach to the tricritical point at $T/T_c \simeq 0.955 \pm 0.005$. The curve is a guide to the eye, based on the explicit example discussed in Ref. 23. The symbols denote the systems studied (only the lowest-temperature value has a numerical error observable on the plotted scale) plus our estimate of the tricritical point. The measured barrier height at $T/T_c = 0.93$ is $(1.0 \pm 0.05) \times 10^{-5} kT_c$. The extrapolation to the tricritical point assumes behavior similar to the work of Ref. 23.

should expect the true tricritical point to lie approximately $(0.025 \pm 0.005) T/T_c$ beyond the temperature at which the barrier height has fallen to $10^{-5} kT_c$. From this we conclude that the tricritical point on the line of wetting transitions obtained from our density-functional theory lies at about $(0.955 \pm 0.005) T/T_c$. Below this temperature, the wetting transition curve of Fig. 8 defines a set of partial wetting wall-vapor profiles that coexist with complete wetting. The behavior of these special partial wetting density profiles is shown in Fig. 10.

Over the entire temperature range covered in our density-functional theory ($T/T_c \geq 0.6$), no hint of first-order behavior was detected along the drying transition boundary. Thus the drying tricritical point, if it exists at all, is predicted by density-functional theory to lie below the triple point of the true Hamiltonian system (or possibly just above it). In addition to the behavior of the grand potential, we found that another route to the position of the equilibrium state in the vicinity of a second-order drying transition is to note the deviations from the force-balance sum rule (17); i.e., the deviation passes through zero very close to the global minimum in the grand potential. Thus we have no reason to doubt the ability of our numerical procedures to faithfully derive the drying transition behavior belonging to the WDA density functional (2). In light of these results it is clearly necessary to reassess the MD computer-simulation data of Ref. 4. In particular, one of the reported indications

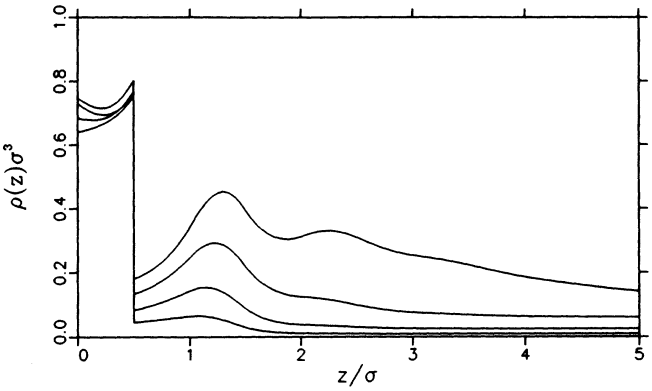

FIG. 10. The interfacial regions of partial wetting wall-vapor density profiles, that coexist with complete wetting along the first-order section of the wetting transition curve, obtained from WDA density-functional theory. The profiles belong to the isotherms $T/T_c = 0.64$, 0.738, 0.85, and 0.93 (in order of increasing vapor density). Inside the range of the wall-fluid potential ($z < \sigma/2$) the $T/T_c = 0.738$ profile is the most dense and the remaining profiles appear in reverse order (highest temperature is least dense).

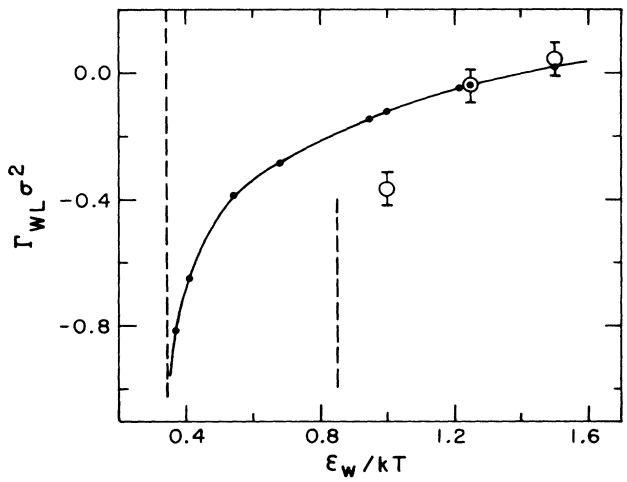

FIG. 11. Comparison between WDA density-functional theory and MD simulation data for an adsorption isotherm at bulk liquid-vapor coexistence, showing a wall-liquid interface approaching complete drying. The comparison is made by choosing (T,μ) such that our density-functional theory gives the same bulk liquid density as obtained from the simulation systems. The points lying on the solid curve (drawn as a guide to the eye) label density-functional results for the isotherm $T/T_c = 0.738$. The open circles with error bars show the simulation results obtained from the profiles plotted in Figs. 1–3. By choosing the abscissa to be ϵ_w/kT, rather than ϵ_w/kT_c, we have avoided any error arising from imprecise knowledge of the simulation value of T_c. The dashed line at $\epsilon_w/kT = 0.344$ denotes the position of the second-order drying transition predicted by our density-functional theory. The dashed line at $\epsilon_w/kT = 0.85$ labels the largest value of ϵ_w for which complete drying was observed in the simulations of Ref. 4.

supporting a first-order drying transition in the simulation study was the sharpness of the transition; for example, in a plot of $n(\sigma/2)-p/kT$ versus $\exp(\epsilon_w/kT)$. In fact, the density functional at the temperature of interest shows a rapid second-order drying transition that is just steep enough to fit into the gap between the two simulation points on either side of the transition. However, there is an unambiguous disagreement over the position of the drying transition. Namely, as one can begin to see in Fig. 3, the wall-liquid partial drying profiles obtained from density-functional theory start to deviate significantly from the simulation results in the region of the simulation drying transition, such that density-functional theory predicts a significantly larger region of partial drying. The above comments concerning the drying transition are summarized by the comparison shown in Fig. 11, which plots wall-liquid adsorptions inside the partial drying region, along the relevant isotherms (i.e., for identical values of the saturated liquid density). From the point of view of Fig. 11, it can now be seen that the MD simulation results are not inconsistent with a second-order drying transition, but that the position of the transition lies at a much larger value of ϵ_w than our density-functional theory predicts. In the light of these surprises, the following section presents a detailed discussion of the problems and weaknesses of the two approaches.

III. WDA DENSITY-FUNCTIONAL THEORY VERSUS MD COMPUTER SIMULATION—DISCUSSION

A. Shared problems

Both methods possess shortcomings associated with the restriction to a finite system size and the neglect of certain fluctuation phenomena. Finite-size effects can be studied by observing the changes that accompany an increase in system size. Computational and numerical efficiency demands the minimum size system compatible with an acceptably small level of finite-size effects. Here, we were significantly helped by the strict finite-range nature of our potentials, (1), but this still leaves effects associated with a loss of fluctuation phenomena. The MD simulation procedure correctly treats short-time fluctuations with wavelengths smaller than the system size, but collective fluctuations (e.g., capillary waves) with periods longer than the total simulation time or with wavelengths too large to fit in the simulation "box" are absent. It is more problematical to assess the situation with regard to density-functional theory; in particular, it is not obvious precisely what damage is being done by the mean-field nature of the grand potential, but only that some fluctuation phenomena are being mistreated.[24] In both approaches it is conceivable that the neglect or mistreatment of fluctuation phenomena could alter the order of a wetting or drying transition.

B. Difficulties with the WDA density-functional theory

Let us concentrate on the nature of the drying transition in our square-well system. Well away from this transition, the density-functional theory shows remarkable agreement with our simulation data, particularly with respect to the density profile. However, this agreement breaks down in the approach to the drying transition. One immediate complication arises from the crudity of the assumed bulk equation of state, (4b). This has arisen from the more general problem concerning the primitive nature of the attractive part of the WDA functional (2); i.e., the second term on the right-hand side of (2a). One might expect the attractive fluid-fluid interactions to play a more important role in determining the structure of a dry interface, in contrast to the oscillatory profiles seen at wet interfaces whose structure is therefore dominated by the packing effects of repulsive fluid-wall and fluid-fluid interactions. Thus one would like to incorporate a more realistic treatment of attractive fluid-fluid interactions into WDA theory, to ascertain whether or not this would remove the predicted shift in the position of the drying transition. One obvious approach, under active consideration at the present time, would be to use WDA theory to evaluate both contributions to the excess free energy; e.g., by adopting the leading-order weight function (9), or the analogous result if a separate coarse-grained density is used to evaluate the attractive fluid-fluid contribution.

In addition, it is prudent, but not obviously of direct relevance to our present discussion, to note that the use of a coarse-grained density makes the grand potential functional highly insensitive to oscillatory structure.[25]

C. Difficulties with the MD simulation procedure

The contrast between the comparison shown in Fig. 3 and that obtained in Figs. 1 and 2 is strong evidence that the MD simulation is unambiguously yielding a drying transition at a significantly higher value of ϵ_w than is predicted by our density-functional theory. On the other hand, the rapid change in structure occurring in the vicinity of the drying transition seen in WDA density-functional theory shows that the MD simulation data are insufficient to base a conclusive judgment on the order of the drying transition observed in Ref. 4. That is, the gap between $0.85<\epsilon_w/kT<1$ is just wide enough to be able to accommodate a second-order drying transition similar to that predicted by density-functional theory. However, the comparison of, say, Fig. 11 shows that only two more simulation data points would be needed to plug the gap; i.e., the density-functional phase behavior, if qualitatively correct, does not present serious difficulties preventing verification by computer simulation. Thus future work is planned to upgrade the simulation data of Ref. 4.

Reference 4 reports direct observations supporting a first-order drying transition that need to be reexamined in the light of the above discussion. In particular, the simulation runs close to the drying transition showed strong signs of metastability and the profile structure was observed to collapse catastrophically when crossing the transition. Although these observations are clearly significant, caution is demanded by the nonequilibrium procedure used to set up the initial unequilibrated simulation systems; namely, the systems were generated by re-

ducing the value of ϵ_w in a series of steps, equilibrating after each step. This procedure could turn second-order behavior into pseudo-first-order behavior, by pushing the system beyond the second-order drying transition. However, since we now know precisely where to look for a possible second-order drying transition, there does not appear to be any problem preventing a definitive simulation experiment.

IV. CONCLUSIONS

This paper has presented a direct comparison between the prediction of WDA density-functional theory and MD computer-simulation data for the nature of a drying transition. In addition, the density-functional theory has been used to map out the global wetting phase diagram for square-well fluid adsorbed at a square-well wall, to facilitate more extensive comparison at a later date. This preliminary comparison has enabled us to learn much concerning the strengths and weaknesses of both approaches, without being able to definitively test one set of results against the other. Two apparently straightforward but time-consuming extensions of this work are called for. (i) Additional MD simulation data are required close to the drying transition of Ref. 4, to test for second-order behavior within a transition region of the size predicted by density-functional theory. Also of some interest would be a simulation study of the wetting transition region of the same isotherm, to confirm the likelihood that MD simulation would presumably agree with the first-order wetting prediction of density-functional theory. (ii) Modification of our density-functional theory to take better account of the role of attractive fluid-fluid interactions is needed to test for possible large effects on the nature and position of drying transitions. For example, by making use of (9) and comparing results with the density-functional theory used above; e.g., Fig. 3. At least one would then be able to use the correct bulk fluid equation of state.[7] We have recently begun work on these extensions.

ACKNOWLEDGMENTS

We owe special thanks to Dr. P. Tarazona for supplying us with a copy of his WDA density-functional program. We also thank Dr. G. Jackson for helpful discussions. Part of the computational work published here was carried out in the School of Chemical Engineering at Cornell University, with the kind permission of Professor K. E. Gubbins. This work was supported by a NATO collaborative research grant.

[1]H. Nakanishi and M. E. Fisher, Phys. Rev. Lett. **49**, 1565 (1982).

[2]D. J. Durian and C. Franck, Phys. Rev. Lett. **59**, 555 (1987).

[3]For general reviews see (a) R. Pandit, M. Schick, and M. Wortis, Phys. Rev. B **26**, 5112 (1982); (b) M. R. Moldover and J. W. Schmidt, Physica D. **12**, 351 (1984); (c) D. E. Sullivan and M. M. Telo da Gama, in *Fluid Interfacial Phenomena,* edited by C. A. Croxton (Wiley, New York, 1986); (d) P. G. de Gennes, Rev. Mod. Phys. **57**, 827 (1985); (e) M. E. Fisher, J. Chem. Soc. Faraday Trans. II **82**, 1569 (1986); (f) S. Dietrich, in *Phase Transitions and Critical Phenomena,* edited by C. Domb and J. Lebowitz (Academic, London, 1988), Vol. 12; (g) R. Lipowsky, Habilitations-Schrift, Ludwig-Maximillians-Universität, München, 1987 (unpublished).

[4]F. van Swol and J. R. Henderson, J. Chem. Soc. Faraday Trans. II **82**, 1685 (1986); for a discussion of grand potential profiles, see J.R. Henderson and F. van Swol, J. Chem. Phys. **89**, 5010 (1988).

[5]J. H. Sikkenk, J. O. Indekeu, J. M. J. van Leeuwen, and E. O. Vossnack, Phys. Rev. Lett. **59**, 98 (1987).

[6]F. van Swol, Phys. Rev. Lett. **60**, 239 (1988).

[7]J. R. Henderson and F. van Swol, Mol. Phys. **56**, 1313 (1985).

[8]M. E. Fisher, J. Chem. Soc. Faraday Trans. II **82**, 1828 (1986).

[9]N. D. Mermin, Phys. Rev. **137**, A1441 (1965).

[10]For a recent review see T. K. Vanderlick, L. E. Scriven, and H. T. Davis, J. Chem. Phys. **90**, 2422 (1989).

[11]J. K. Percus, J. Chem. Phys. **75**, 1316 (1981).

[12]T. F. Meister and D. M. Kroll, Phys. Rev. A **31**, 4055 (1985).

[13](a) W. A. Curtin and N. W. Ashcroft, Phys. Rev. A **32**, 2909 (1985); (b) Phys. Rev. Lett. **56**, 2775 (1986).

[14]P. Tarazona, Phys. Rev. A **31**, 2672 (1985).

[15]T. K. Vanderlick, L. E. Scriven, and H. T. Davis, J. Chem. Phys. **85**, 6699 (1986).

[16]A series of proofreading errors resulted in a string of incorrectly published results for the coefficients w_i. The actual values used in the program can be found in the appendix to P. Tarazona, U. Marini Bettolo Marconi, and R. Evans, Mol. Phys. **60**, 573 (1987).

[17]J. R. Henderson, Mol. Phys. **59**, 1049 (1986); Phys. Rev. B **35**, 7303 (1987); Mol. Phys. **62**, 829 (1987).

[18]P. Schofield and J. R. Henderson, Proc. R. Soc. (London), Ser. A **379**, 231 (1982).

[19]J. R. Henderson, Mol. Phys. **48**, 715 (1983); **50**, 741 (1983).

[20]The simulation systems lie on an isotherm $T/T_c \simeq 0.775$, assuming the estimate of T_c given by B. J. Alder, D. A. Young, and M. A. Mark, J. Chem. Phys. **56**, 3013 (1972).

[21]The explicit formulas involved are

$$\Omega_{WV}^{(s)}\sigma^2/kTA = \tfrac{1}{4}(p\sigma/kT)^2 h_2 + \tfrac{1}{8}\rho_w(\rho_w - p/kT)[h_0\sigma^4 + \tfrac{1}{8}\pi\sigma^6] - \tfrac{1}{2}(\rho_w - p/kT)\sigma^3$$

together with

$$\rho_w kT = p\{1 + [\exp(-\epsilon_w/kT) - 1] \times \exp[\tfrac{1}{2}(p/kT)(h_0\sigma + \pi\sigma^3/12)]\}^{-1},$$

$$h_0 = (\pi/4)[5\exp(\epsilon/kT) - 9],$$

$$h_2 = (\pi/32)[65\exp(\epsilon/kT) - 81].$$

These expressions are obtained from a sum rule for the surface excess grand potential (the first formula) and a sum rule for the density-profile gradient [which is integrated and combined with (17) to give the second formula] in the weak-gas limit for the total correlation function; $g(12) - 1 \rightarrow \exp[-u(r)/kT] - 1$, whose first and third moments (the

expressions for h_0 and h_2) determine the sum rules. The exact versions of the sum rules can be found, for example, in Ref. 7. The values of $\Omega_{wv}^{(s)}$ and hence $\cos\theta$ given in Ref. 4, obtained from the above expressions, contain a slight error. The values of $\cos\theta$ that should have appeared in Table 1 of Ref. 4 are -1.06, -0.52, and -0.21.

[22]P. Tarazona and R. Evans, Mol. Phys. **48**, 799 (1983).

[23]T. Aukrust and E. H. Hauge, Physica A **141**, 427 (1987).

[24]R. Evans, Mol. Phys. **42**, 1169 (1981).

[25]In particular, at moderate to low temperature well above the triple point of the square-well Hamiltonian system, we noticed that WDA density-functional theory yields apparently stable (given a careful choice of mixing parameter) weak oscillatory structure on the bulk liquid side of the liquid-vapor interfacial profile. These wiggles grow as the temperature is lowered and remain localized to the liquid side of the interface if one doubles the system length. Furthermore, we observed that the original density-functional program predicts similar oscillations in the liquid-vapor profile of a Yukawa fluid. These oscillations are smaller at a corresponding temperature than for the square-well system because Yukawa fluid-fluid interactions are anomalously soft and thus mimic a higher temperature (i.e., lead to a thicker liquid-vapor profile), which presumably explains why this peculiar behavior has not been reported previously. Clearly, one would not want to give much physical significance to these oscillatory liquid-vapor profiles, even when taking into account the mean-field nature of the theory.